International Journal of Basic Science and Technology
May, Volume 11, Number 2, Pages 93 - 106 http://www.ijbst.fuotuoke.edu.ng /93
https://10.5281/zenodo.15363231 ISSN 2488-8648

Reservoir Characterization and Prospectivity Studies Using Well Logs and Seismic Data in ENF Field Onshore Niger Delta, Nigeria

[1]Erugba F. N and [2]Acra E. J
[1] Center for Petroleum Geoscience, Faculty of Engineering, University of Port Harcourt, Nigeria.
[2]Department of Geology, Faculty of Science, University of Port Harcourt, Nigeria

Article Information

Article # 100263
Received: 4th March. 2025
Revision:9th April. 2025
2nd Revision:19thApril. 2025
Acceptance 3nd May 2025
Available online:
9th May, 2025.

Key Words
Maximum Amplitude,
Water saturation,
Permeability
Porosity,
Density.

Abstract

The ENF field is located within latitudes 4°50'42.36N to 4°56'43.35N and longitude 6°15'54.99E to 6°27'24.71E in Niger Delta. Reservoir characterization involved the quantitative distribution of petrophysical parameters (porosity, permeability, net-to-gross, water saturation) derived from log interpretation within a particular reservoir sand interval, while prospectivity studies involve the evaluation of ENF field for more prospects and leads. Well logs (density, neutron, GR, resistivity and sonic) were utilized for this study. Well correlation was done across seven wells, and three reservoir sands of interest (sand A, C and I) were picked using GR and resistivity. The reservoir sand thickness for A, C, and I were 404.32, 306.65 and 193.86, respectively, with a very good porosity and permeability of (0.25, 0.27, 0.19) and (1098.21mD, 1585.81mD, 850.17mD) Seismic data were thoroughly interpreted and a time surface map was generated. The velocity model was carried out, which helped in time depth conversion (converting time surface map to depth surface). The fault within the ENF field was modelled utilizing the top and base depth surface map, and the major fault served as a boundary to pillar grid the reservoir sands. The volume of hydrocarbon was calculated for each reservoir, and the result showed that reservoir A has 411MMSTB (Million Stock Tank Barrels), reservoir C 654MMSTB while reservoir I has 1351MMSTB. the field was evaluated for more prospect and leads utilizing seismic attributes (RMS and maximum amplitude). The bright spot amplitude anomalies showed that there is hydrocarbon. Therefore, more wells should be drilled within the prospect for optimal recovery of hydrocarbon.

*Corresponding Author: Acra E. J.; edward.acra@uniport.edu.org

Introduction

In the petroleum industry, the characterizing of a potential reservoir is the most expensive cost item in the spectrum of geophysical activities. To have a good characterized reservoir means a high rate of success and few wells for the production of hydrocarbon. Reservoir characterization is the distribution of parameters (porosity, permeability, water saturation, Net-to-gross) quantitatively within a defined gridded reservoir interval.

Using resistivity logs and GR logs to characterize a reservoir is more precise (Asquith, 2004). Deterministic and linear methods are effective technique that helps to estimate what is happening within the subsurface and the response from seismic (Michele *et al*., 2015). Well log interpretation is crucial in characterizing a reservoir because it helps you to get the required petrophysical properties. Seismic data acquired in Niger Delta reveals how many structures that results from deltaic tectonic. The structures seen in the Niger Delta includes: growth faults (i.e. defined by fault plane that are concave). Another geologic structure is a roll-over anticline that can be related to a growth fault. This study aims to properly characterize a reservoir and prospectivity studies using well- logs and seismic volume. The objectives were strictly followed to achieve the delineation of reservoir units, well-to-well correlation of reservoir units. Seismic-well-tie using Gardner's equation, seismic interpretation (fault and horizon mapping). Generation of time and depth surface maps and petrophysical evaluation and estimation of NTG (Net-to-Gross ratio) of the respective reservoir intervals, and volumetric calculation.

Location of Study Area

The "ENF" Field is situated in Bayelsa State, Central Swamp. The field is bounded geographically by latitude 4°50′42.3642″N to 4°56′43.3537″N and longitude 6°15′54.9938″E to 6°27′24.7090″E (Figure 1) The ENF field is about 4*6 kilometres in aerial extent.

https://10.5281/zenodo.15363231 ISSN 2488-8648

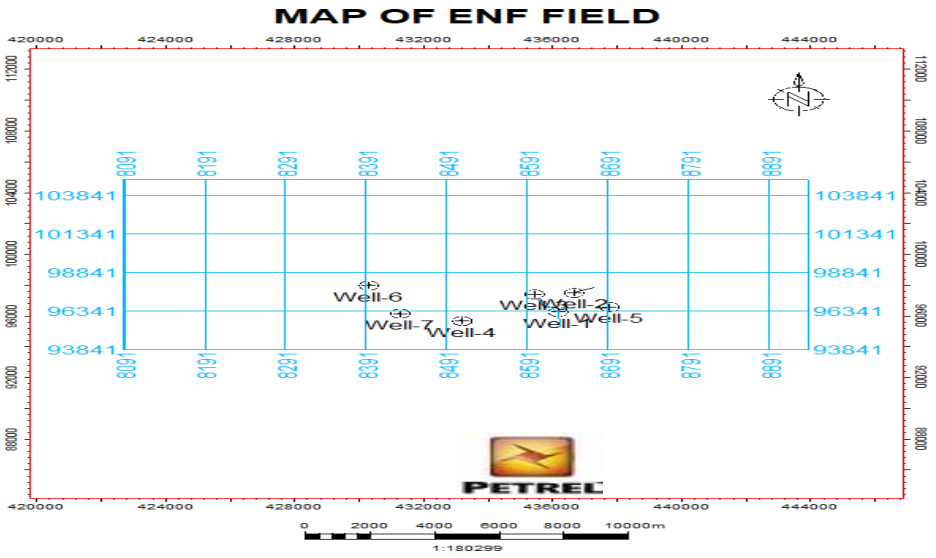

Figure 1: Base map of the study area

Niger Delta lithostratigraphic framework

According to Omatsola and Knox 1989, the outbuilding of the Delta gave rise to a different successive growth that is called depobelt (Figure 2). Notwithstanding the particular depobelts, Niger Delta Province is composed of three (3) Formations; starting from the oldest we have the Akata Formation, the Agbada Formation and the Continental sand of the Benin Formation (Reijers, 2011).

Akata Fromation

Akata Formation is the ancient stratigraphic unit in the Niger Delta basin which is at the bottom end of the entire Delta (Weber and Daukoru, 1975). From literature, the Akata Formation consist of marine shales (Doust and Omatsola, 1989), with little deep water turbidite sands (Beka and Oti, 1995) and minor silt. During transportation of sediments, clay materials and organic matter were carried and deposited in the deep ocean, where there is low energy and anoxic environment (Stacher, 1995) of a thickness of seven (7) kilometers (Doust and Omatsola, 1990).

Agbada Formation

This Formation in the Niger Delta basin is on-top of the Akata and it is considered the second stratigraphic unit of the Niger Delta basin. Sediment deposition and accumulation happened from the Eocene to the Present. The Agbada is the reservoir sand that host hydrocarbon resources of the Niger Delta. The intercalations of shales with varying thickness which interrupt the sand are believed to serve as the seal/cap rock, which makes the entrapment of hydrocarbon possible (Short and Stauble, 1967; Ejedawe, 1989). The lower Agbada Formation is believed to be a majorly shale body, while the upper Agbada is a majorly sand and a framework of intercalations of shale (Avbovbo, 1978). Structural framework of the Agbada Formation includes the roll-over anticline, collapse crest and growth fault (Xiao and Suppe, 1992).

Benin Formation

This Benin Formation is agreed to be the most recent formation in the Niger Delta. It is underlined by the Agbada. It consists predominantly of continental & coastal plain sand-deposits with little silt, shale and small clay deposits. Sediment deposits in the Benin Formation from the Eocene to present age. The sand grain sizes range from coarse-grained to fine-grained, moderate sorted. The sediment is about 2000 meters in thickness, and it varies from one locality to another (Avbovbo, 1978).

https://10.5281/zenodo.15363231 ISSN 2488-8648

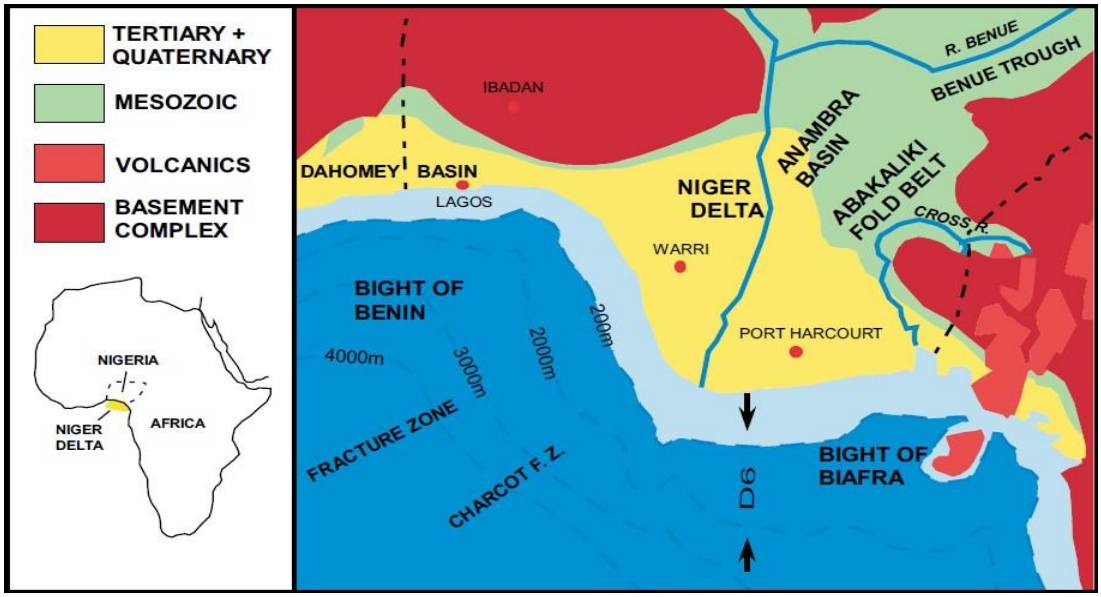

Figure 2: Niger Delta map by Doust and Omatsola 1989

Tectonic Setting of the Niger Delta

Tectonic framework of Niger Delta is made up of basically an extensional rift basin which is associated with shale diapers due to compressional stress. Another style of deformation is attributed to gravitational basin collapse resulting in shale diapirism and slope instability because of inadequate support for the Akata shale that is under-compacted (Michele *et al.*, 2015). The Niger Delta Province have three zones structurally (extensional, compressional and transitional zone) which shows a series of structural styles that were found around the Delta. The geologic structure found in this delta is mainly the syn-depositional growth fault, collapse crest structures, roll-over anticline and shale diapars which defined the delta structurally (Evamy, *et al.*, 1978). These structural complexities are concentrated in the middle and reduce toward the flank, implying that the delta flank is relatively quiet, and this explains why the hydrocarbon traps seen in the flanks are mainly stratigraphic (Beka and Oti, 1995).

Materials and Methods

This study utilized a comprehensive dataset (Table 1) comprising a 3D seismic volume, well logs (sonic, neutron, density, gamma ray, and resistivity), a base map, a checkshot survey (available for Well 1 only), and deviation survey data. The seismic volume spans an area of approximately 840 km². Data processing and analysis were conducted using Petrel and Microsoft Excel software. Well logs and checkshot data were exported in ASCII format, while seismic data were provided in SEGY format. The methodology is structured as follows:

Data Acquisition: The dataset was acquired, including a 3D seismic volume covering 840 km², well logs (sonic, neutron, density, gamma ray, and resistivity), a base map, checkshot data for Well 1, and deviation survey data. All data were verified for quality and completeness to ensure suitability for subsequent analysis.

Correlation: Well logs were correlated across the study area using gamma ray and resistivity logs to establish stratigraphic and structural continuity. The checkshot data from Well 1 were used to calibrate the time-depth relationship, while deviation survey data aided in accurate well trajectory mapping. The base map facilitated spatial alignment of wells and seismic data.

Interpretation: The 3D seismic volume was interpreted to identify key horizons and faults, guided by well log correlations. Seismic attributes, such as amplitude and coherence, were analyzed to delineate reservoir boundaries and facies variations. Well log data were interpreted to determine lithology, porosity, and fluid content, integrating sonic, neutron, and density logs for petrophysical characterization.

Modeling: A 3D geological model was constructed using Petrel, incorporating interpreted seismic horizons, faults, and well log-derived properties. The

https://10.5281/zenodo.15363231 ISSN 2488-8648

model integrated structural and stratigraphic frameworks, with petrophysical properties distributed across the reservoir zones. Time-depth conversion was refined using checkshot data to ensure accuracy.

Volumetric Analysis: Volumetric calculations were performed within the 3D model to estimate hydrocarbon in-place volumes. Key parameters, including reservoir thickness, porosity, and saturation, were derived from well log interpretations. Microsoft Excel was used to validate calculations and assess uncertainties in volume estimates.

Prospectivity Evaluation: The prospectivity of the reservoir was evaluated by integrating seismic, well log, and volumetric data. Reservoir quality was assessed based on porosity, permeability, and connectivity derived from the model. Seismic attributes and fault analysis were used to identify potential hydrocarbon traps and migration pathways, ranking prospects based on risk and resource potential.

Table .1: Available data utilized

WELL NAME		1	2	3	4	5	6	7
WELL HEADER		√	√	√	√	√	√	√
WELL LOGS	GR (GAPI)	√	√	√	√	√	√	√
	RT (Ohm.m)	√	√	√	√	√	√	√
	NPHI (m^3/m^3)	√	√	–	√	√	√	√
	RHOB (g/cm^3)	√	√	√	√	√	√	√
	DT (µs/ft)	√	–	–	–	–	–	–
WELL DEVIATION		√	√	√	√	√	√	√
CHECKSHOT		√	–	–	–	–	–	–

Results and Interpretation

Results of Reservoir Characterization

Three reservoirs were identified during this work regarding hydrocarbon occurrences. The petrophysical properties that were calculated include permeability, Φ, Sw, NTG, and Vsh. The petrophysical results for the three reservoirs are presented below in Tables 3, 4 and 5.

https://10.5281/zenodo.15363231 ISSN 2488-8648

Table 2: Result of petrophysical parameter for reservoir sand A

WELLS	TOP (ft)	BASE (ft)	THICKNESS (ft)	OWC (ft)	ΦT	ΦE	K(mD)	Sw	NTG	VSH
1	7185.41	7640.32	454.91	–	0.3	0.23	919.75	0.53	0.74	0.24
2	6964.79	7316.16	351.37	–	–	–	–	0.43	–	0.16
3	7051.93	7449.64	397.71	–	0.28	0.25	1221.45	0.42	0.87	0.12
4	6978.38	7400.61	422.23	–	–	–	–	0.47	–	0.23
5	7090.06	7515.02	424.96	–	0.33	0.27	1153.42	0.5	0.8	0.21
6	7005.62	7427.85	422.23	–	–	–	–	0.45	–	0.24
7	7193.58	7550.43	356.85	–	–	–	–	0.54	–	0.25

Table 3:Results of petrophysics parameters for the reservoir sand C

WELLS	TOP (ft)	BASE (ft)	THICKNESS (ft)	OWC (ft)	ΦT	ΦE	K(mD)	Sw	NTG	VSH
1	8457.55	8615.54	157.99	–	0.29	0.26	1371.17	0.41	0.91	0.11
2	8016.25	8313.17	296.92	–	–	–	–	0.39	–	0.07
3	8239.62	8582.85	343.23	–	0.28	0.27	1730.83	0.35	0.95	0.05
4	8106.14	8443.93	337.79	–	–	–	–	0.39	–	0.07
5	8277.76	8615.54	337.78	–	0.32	0.29	1655.43	0.4	0.93	0.12
6	8117.04	8419.41	302.37	–	–	–	–	0.45	–	0.08
7	8394.89	8765.37	370.48	–	–	–	–	0.44	–	0.24

Table 4: Result of petrophysical parameters for reservoirs sand I

WELLS	TOP (ft)	BASE (ft)	THICKNESS(ft)	OWC (ft)	ΦT	ΦE	K(mD)	Sw	NTG	VSH
1	11689.59	11907.52	217.93	11899.35	0.24	0.13	566.97	0.3	0.4	0.5
2	11558.39	11754.97	196.58	11787.66	0.37	0.32	1544.69	0.17	0.81	0.18
3	11828.52	12065.51	236.99	12090.03	0.3	0.26	1211.13	0.2	0.75	0.16
4	11648.73	11833.97	185.24	11828.52	0.23	0.17	721.08	0.22	0.63	0.33
5	11872.1	12051.89	179.79	11902.07	0.21	0.18	648.67	0.63	0.84	0.18
6	11602.42	11787.66	185.24	11787.66	0.25	0.19	772.17	0.25	0.68	0.31
	11569.73	11725.01	155.28	11727.73	0.19	0.11	486.5	0.29	0.4	0.56

3Structural interpretation

A fault line was first drawn on the variance volume attribute (Figure 3.1) before it was picked on the seismic as presented in Figure 4.2. Seventeen faults were found across the section. A seismic-well-tie was done, and horizons were mapped across; a seed grid was generated for the three reservoir sand tops (Figure 3.3, 3.4 and 3.5). A fault polygon was generated (Figure 3.6). Then the seed grids generated were used for 3D auto tracking, which was further used for time surface generation for sand A, C and I surfaces (Figure 3.7, 3.8 and 3.9, respectively). The time-depth relationship model was used for time-depth conversion.

https://10.5281/zenodo.15363231 ISSN 2488-8648

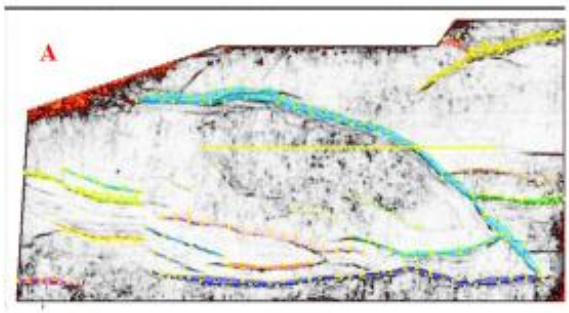

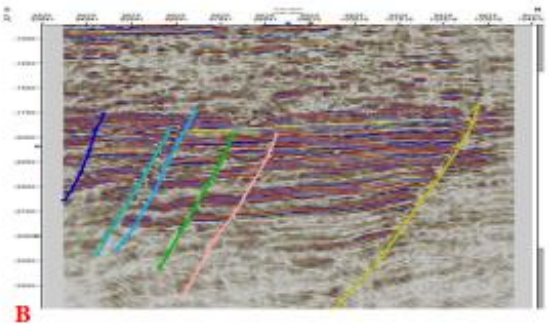

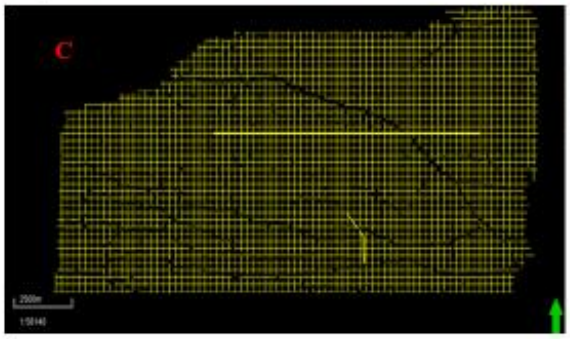

Figure 3.1A: Fault line on variance seismic volume attribute.
Figure 3.2B: Fault line on Seismic section
Figure 4.3C: Seed greed generated for reservoir top A

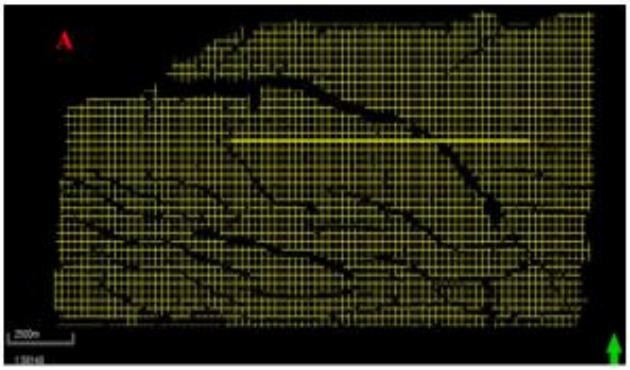

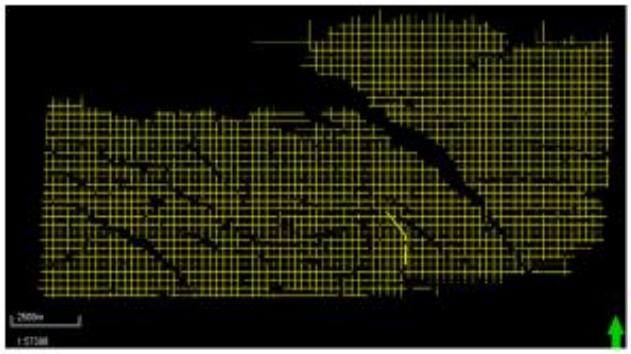

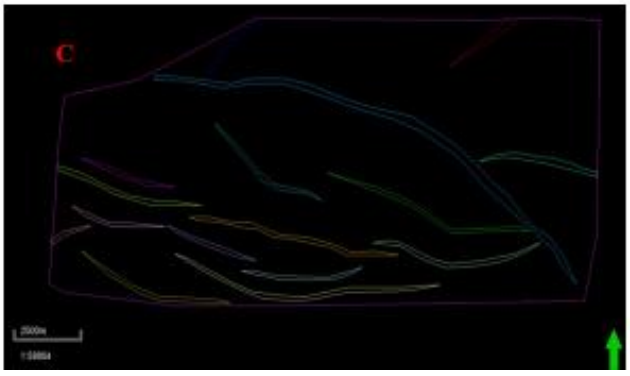

Figure 3.4A: Seed greed generated for reservoir top C
Figure 3.5B: Seed greed generated for reservoir top I
Figure 3.6C: Fault Polygon

https://10.5281/zenodo.15363231 ISSN 2488-8648

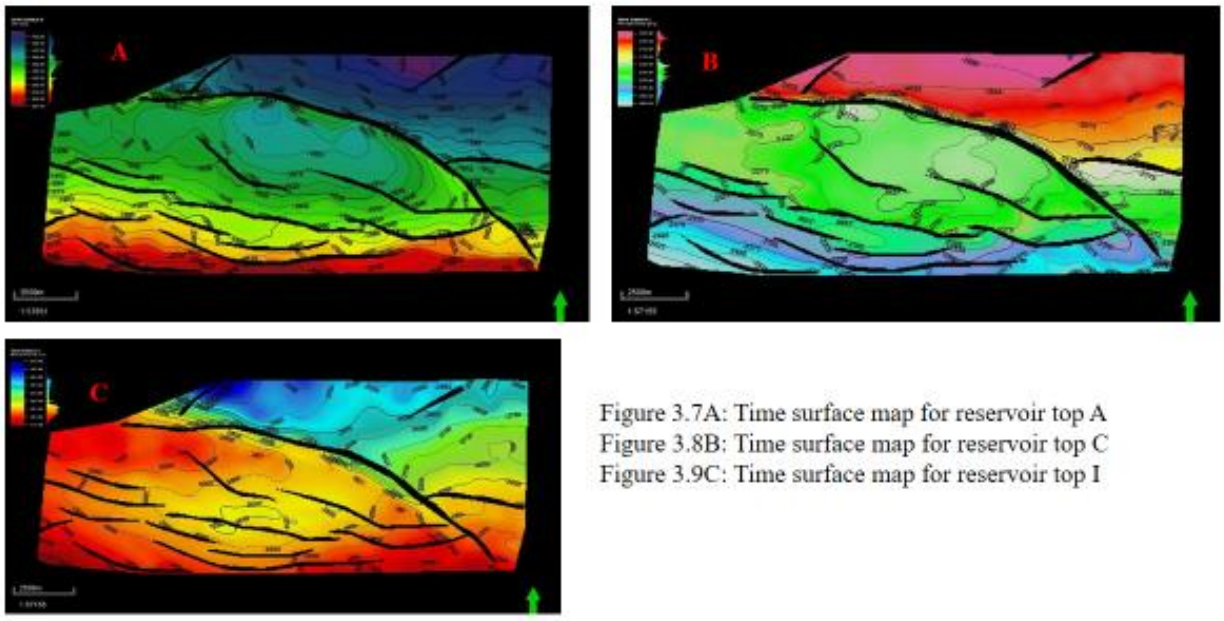

Figure 3.7A: Time surface map for reservoir top A
Figure 3.8B: Time surface map for reservoir top C
Figure 3.9C: Time surface map for reservoir top I

Depth surface map generation

A velocity models were obtained from plotting time-depth-relationship (TDR) against two-way-time (TWT) on a function window (Figure 3.4) with a non-linear polynomial function to have a velocity equation. The velocity equation was utilized in changing the time map generated to a depth map (Figures 3.11, 3.12 and 3.13) for each of the reservoir sands by using a lookup function from Petrel. Both the time and depth surface structural maps revealed that the three reservoirs were trapped in an anticlinal structure and the identified closures are fault-controlled

.

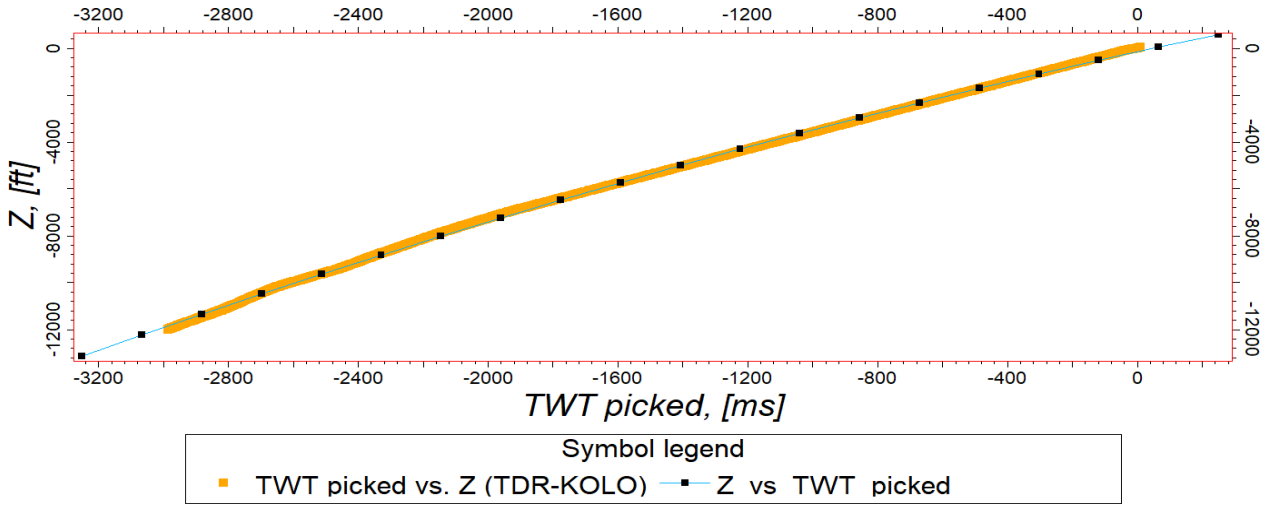

Figure 3.4: A plot of Z (depth) against two-way-time

https://10.5281/zenodo.15363231 ISSN 2488-8648

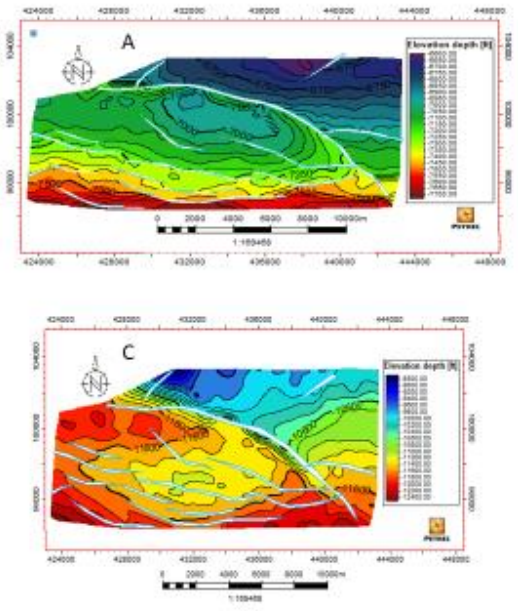

Figure 3.11A: Depth surface map on reservoir top A
Figure 3.12B: Depth surface map on reservoir top C
Figure 3.13C: Depth surface map on reservoir top I

Reservoir thickness

Using gamma ray log, the top and base of sands A, C and I were mapped across the seven wells available. Then both gamma ray log and resistivity logs were utilized and three reservoirs of interest (Table 5) were picked for horizon mapping (Rivenæs *et al.*, 2015). The top and base of the three reservoirs of interest were converted to isochore points and utilized for generating a thickness map for the three reservoirs A, C and I as seen in Figure 3.14, 3.15 and 3.16, respectively (Emujakporue, 2017).

Table 5: Reservoir tops and base

SAND A							
WELLS	1	2	3	4	5	6	7
TOP (ft)	7185.41	6964.79	7051.93	6978.38	7090.06	7005.62	7193.58
BASE (ft)	7640.32	7316.16	7449.64	7400.61	7515.02	7427.85	7550.43

SAND C							
WELLS	1	2	3	4	5	6	7
TOP (ft)	8457.55	8016.25	8239.62	8106.14	8277.76	8117.04	8394.89
BASE (ft)	8615.54	8313.17	8582.85	8443.93	8615.54	8419.41	8765.37

SAND I							
WELLS	1	2	3	4	5	6	7
TOP (ft)	11689.59	11558.39	11828.52	11648.73	11872.1	11602.42	11569.73
BASE (ft)	11907.52	11754.97	12065.51	11833.97	12051.89	11787.66	11725.01

https://10.5281/zenodo.15363231 ISSN 2488-8648

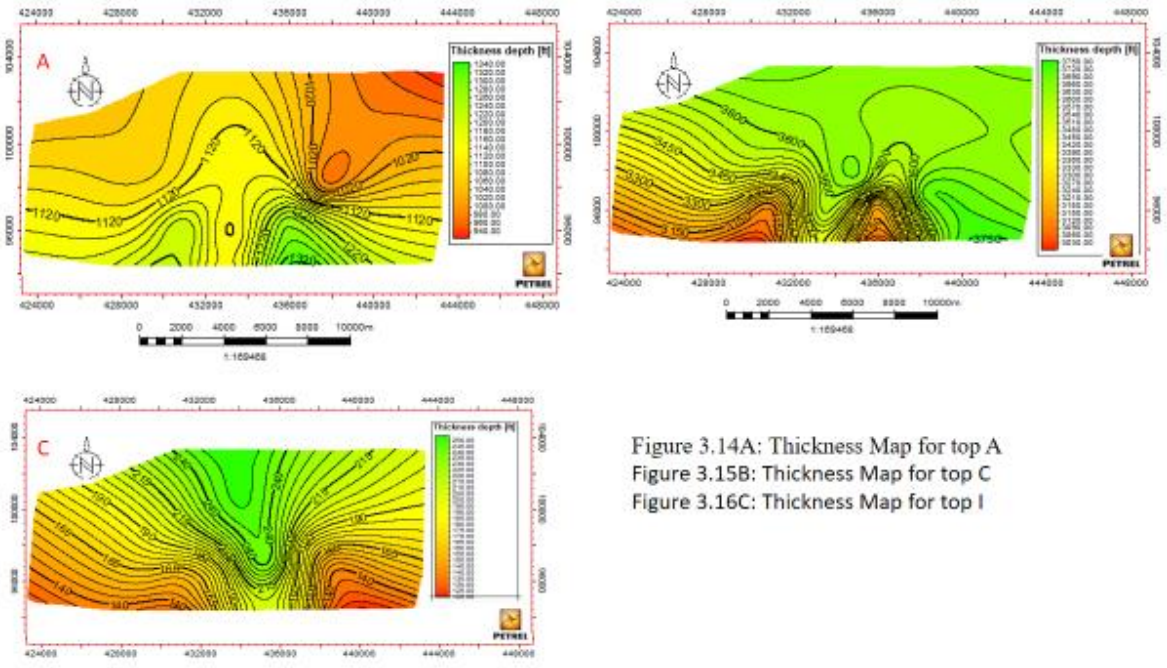

Figure 3.14A: Thickness Map for top A
Figure 3.15B: Thickness Map for top C
Figure 3.16C: Thickness Map for top I

Results of static modelling

From the model, the fault polygons generated were modelled (Figure 3.17) and adjusted properly to fit into the depth surface for each of the reservoirs. The modelled faults were used as a boundary to generate a pillar grid.

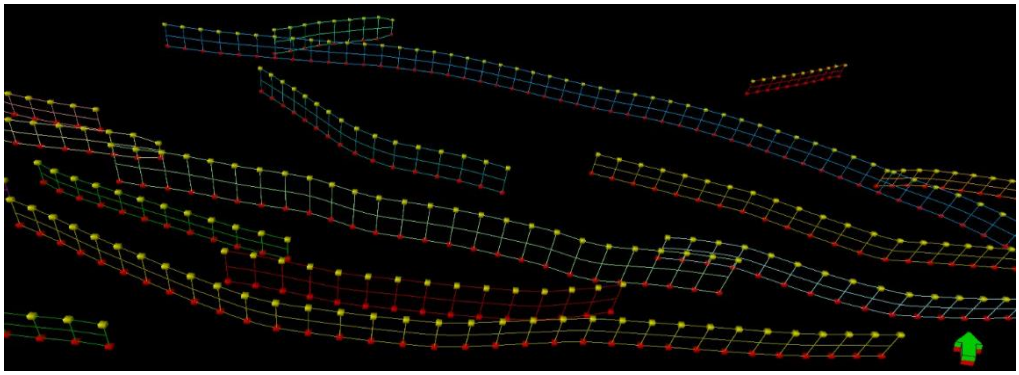

Figure 3.17: Fault polygon

Results of fluid contact

A contact between the hydrocarbon and water was established based on GR log and the resistivity log. Neutron-density log was utilized to get the type of fluid (Duvbiama *et al*., 2017). The reservoir sand of A, C and I were identified to contain oil and water, which was based on petrophysical evaluation. Fluid contact was established for wells in reservoir sand A and C (Figure 3.18) because their resistivity was flat (i.e. no resistivity kick to indicate hydrocarbon presence). But in the reservoir sand I, hydrocarbon water contact was identified (Figure 3.19). From the fluid contact surface generated for reservoirs and A and C, it showed that the reservoir is mostly water with little oil present (Figures 3.20 and 3.21, respectively). Then in the reservoir sand I the fluid contact surface showed that there is a presence of OWC. The oil-water contact map for the reservoir sand I explained that the wells were drilled into the hydrocarbon zone (Figure 3.22).

https://10.5281/zenodo.15363231 ISSN 2488-8648

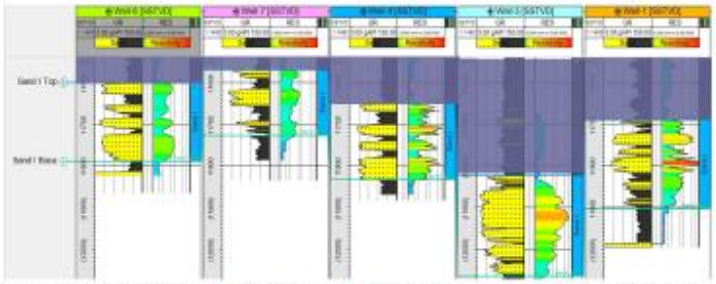

Figure 3.18: GR log and Resistivity log showing fluid contact for reservoir sand A and C

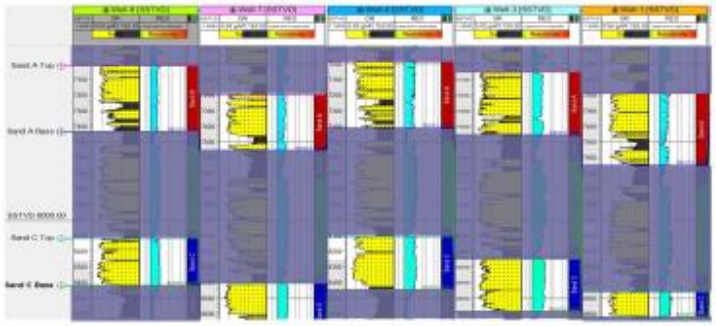

Figure 3.19: GR log and Resistivity log showing fluid contact for reservoir sand I

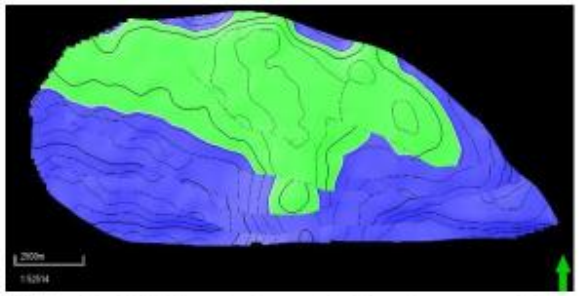

Figure 3.20: Fluid contact for sand A showing water and little oil

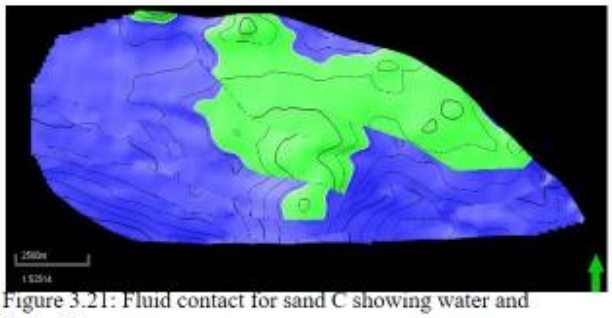

Figure 3.21: Fluid contact for sand C showing water and little oil

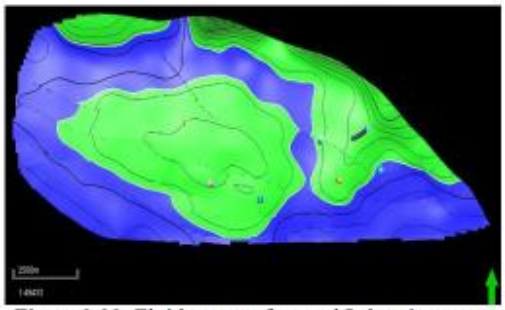

Figure 3.22: Fluid contact for sand I showing water and oil and the drilled wells

Result of petrophysical modelling

Facies model for reservoir A is (sand 65.63%, fine sand 1.31%, coarse sand 5.74, shale 27.32), reservoir C (sand 83.64, fine sand 3.13, coarse sand 4.19 and shale 9.04) and reservoir I (sand 50.92, fine sand 3.73, coarse sand 8.36 and shale 36.99). Figure 3.23a.b and 3.25 show a modelled property of facies, water saturation and permeability for the three reservoirs, respectively. In comparison, where we have coarse sand and sand is where we have a very good porosity and permeability with very little water saturation, and this helps to explain the heterogeneity of the lithofacies (Aigbadon *et al*., 2017). The

https://10.5281/zenodo.15363231 ISSN 2488-8648

recommendation for more wells to be drilled is based on the volumetric data obtained from the Petrel software.

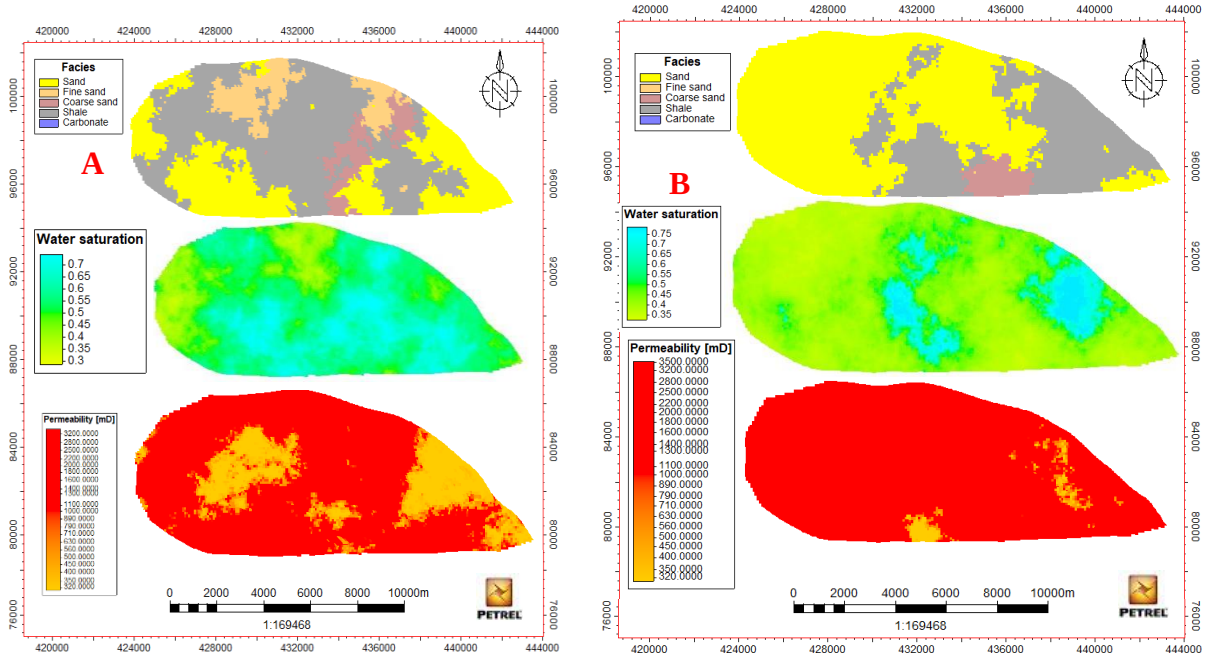

Figure 3.23A and B: Modelled petrophysical parameters for reservoir A and Modelled petrophysical parameters for reservoir C

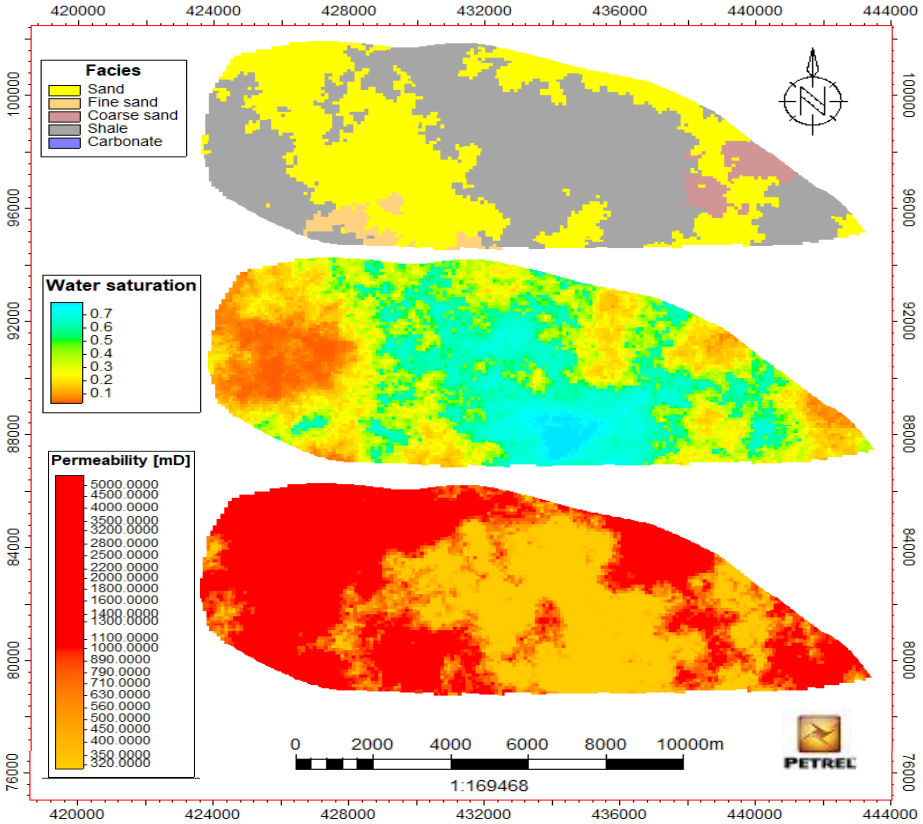

Figure 3.25: Modelled petrophysical parameters for reservoir A

https://10.5281/zenodo.15363231 ISSN 2488-8648

Prospect evaluation

The seismic attributes utilized are maximum amplitude, Root Mean Square and sweetness. The maximum amplitude and RMS surface attribute showed hydrocarbon prospective areas with good quality sand (Figure 3.26 to 3.31), respectively (Uwem *et al*., 2018). The bright amplitude anomalies give an indication of hydrocarbon presence and also the quality of the reservoir sands. The prospect area has an anticlinal closure system that is closed by the major fault and other minor faults in the field. Also, a lead was identified which lies on the upthrow block of the fault's block and was separated by the major fault. The oil water contact map for reservoir "I" explained that the hydrocarbon bearing zone are large enough and this validates the bright spot established by Root Mean Square attribute and Maximum Amplitude seismic attributes in Figure 3.30 and 3.31 for reservoir sand I. from all indication, the Root Mean Square interpretation is more reliable because it gives more indication of where we have bright spot (Nwankwo *et al.*, 2014).

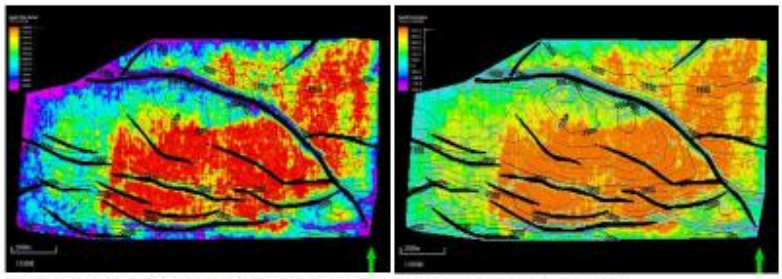

Figure 3.26: RMS amplitude seismic attribute for reservoir sand A
Figure 3.27: Maximum amplitude seismic attribute for reservoir sand A

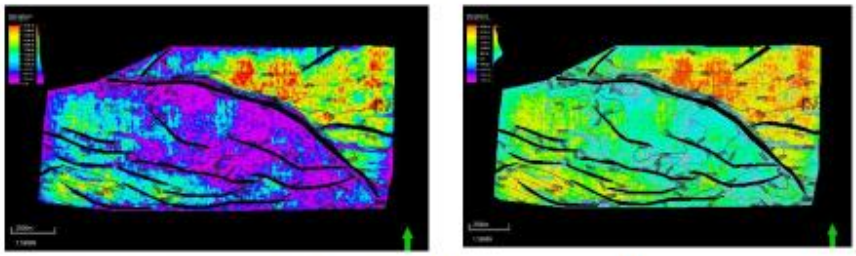

Figure 3.28: RMS amplitude seismic attribute for reservoir sand C
Figure 3.29: Maximum amplitude seismic attribute for reservoir sand C

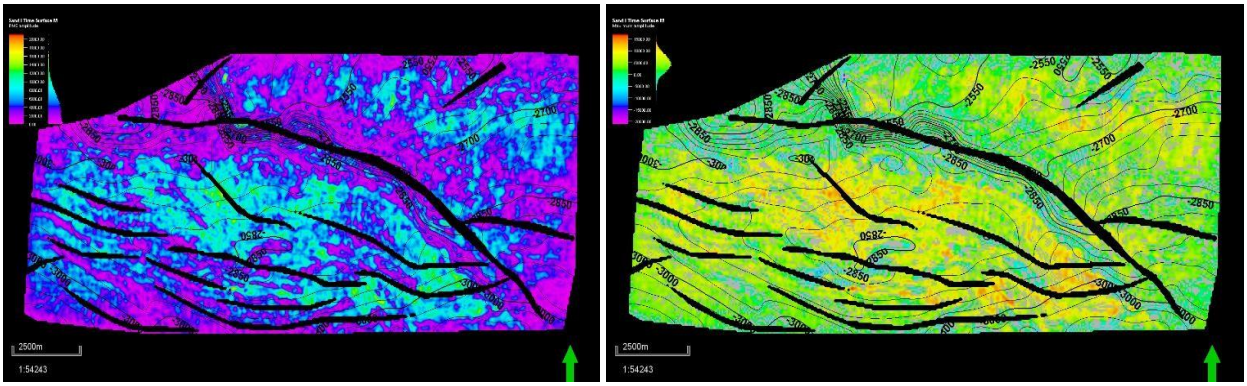

Figure 3.30: RMS amplitude seismic attribute for reservoir sand I
Figure 3.31: Maximum amplitude seismic attribute for reservoir sand I

https://10.5281/zenodo.15363231 ISSN 2488-8648

Volumetrics Interpretation

The volume of HC was calculated for the reservoir-sand A, C and I. The result of the volume of HC is presented in Table 6.

Table 6: Showing Volumetrics calculation using Petrel volume calculation

PETROPHYSICAL PARAMETERS	RESERVOIR A	RESERVOIR C	RESERVOIR I
RESERVOIR THICKNESS (ft)	404.32	306.65	193.86
POROSITY effective	0.25	0.27	0.19
WATER SATURATION	0.48	0.4	0.29
NET-TO-GROSS	0.8	0.93	0.64
NET-TO-GROSS	0.8	0.93	0.64
PORE VOLUME (10^6 RB)	1230	1676	2719
BULK VOLUME (10^6 ft^3)	38176	36314	124036
NET VOLUME (10^6 ft^3)	27791	34162	77231
OIL FVF Bo (RB/STB)	1.5	1.5	1.5
RECOVERY FACTOR OIL	1	1	1
STOIIP (10^6 STB)	411	654	1351
RECOVERABLE OIL (10^6 STB)	411	654	1351

Summary and Conclusion

Summary

This project work was done utilizing composite logs & seismic volume to characterize a reservoir and prospectivity studies of ENF field. Seven wells were used for this project: well header, well deviation, composite well logs (GR, resistivity, neutron-density & sonic), seismic volume, and checkshot were made available. The well was correlated across the seven wells using GR log. Three reservoirs of interest were identified utilizing GR log (lithology definition), resistivity log (fluid content) & neutron-density log (for fluid type).

Seismic interpretation, which includes fault picking and horizon tracking, was done using the seismic volume. Faults were picked in the inline along the whole seismic section with an increment of 10 spacing (250m on the ground surface). Seismic-well-tie was done using the provided seismic section, checkshot, density-log, sonic-log and a seismic wavelet generated (Extended white algorithm). The sonic-log was calibrated, and a synthetic seismogram was obtained utilizing Gardner's equation with a time bulk shift of "-5". A synthetic seismogram was generated, then followed by horizon mapping (tracking the well tops correlated) in the crossline and inline. The seed-grid generated was embedded to have a tie surface map for the 3 reservoir sands, and the fault polygon was drawn & used to eliminate the inside from the time surface. A time depth conversion was done using a velocity model. A plot of depth versus two-way-time using a non-linear polynomial function was utilized to get the velocity function. After the velocity-time depth conversion, a depth surface map was generated. Also, seismic attributes (RMS and maximum amplitude) were utilized for prospect identification and the bright spot from these attributes showed the presence of hydrocarbon and also areas that have hydrocarbon. From the Volumetrics calculated, the volume of hydrocarbon for reservoir A is 411MMSTB, reservoir C is 654MMSTB then, reservoir I is 1351MMSTB

Conclusion

From the petrophysical parameters, the result showed that the reservoirs A, C and I have a reservoir sand with thicknesses 404.32, 306.65 and 193.86, respectively, with a very good porosity and permeability of (0.25, 0.27, 0.19 and 1098.21mD, 1585.81mD and 850.17mD) respectively. The structural state of the ENF field explained that the hydrocarbon was trapped

https://10.5281/zenodo.15363231 ISSN 2488-8648

in an anticlinal structure with fault closures. The amplitude anomalies from the seismic attribute revealed that there is a prospect with high volume of hydrocarbon within the field, therefore, 4D seismic should be acquired, and more wells should be drilled in order to evaluate the prospects.

References

Asquith, G., and Krygowski, D. (2004). Basic well log analysis. *AAPG Methods in Exploration, 16*, 1–20.

Avbovbo, A. A. (1978). Tertiary lithostratigraphy of Niger Delta. *American Association of Petroleum Geologists Bulletin, 62*(2), 295–300.

Beka, F. T. and Oti, M. N. (1995). The distal offshore Niger Delta: Frontier prospects of a mature petroleum province. In M. N. Oti & G. Postma (Eds.), *Geology of deltas* (pp. 237–241). Rotterdam: A.A. Balkema.

Doust, H and Omatsola, E. (1990). Niger Delta. In J. D. Edwards & P. A. Santogrossi (Eds.), *Divergent/passive margin basins, AAPG Memoir 48* (pp. 239–248). Tulsa, OK: American Association of Petroleum Geologists.

Duvbiama, O.and Ikomi, J. (2017). 3D static modelling of an offshore field in the Niger-Delta. *SPE Nigeria Annual International Conference and Exhibition*, Lagos, Nigeria, 31 July–2 August.

Ejedawe, J. E. (1989). The eastern Niger Delta: Geological evolution and hydrocarbon occurrences. *SPDC Internal Report, Exploration Note 89.002*.

Emujakporue, G. O. (2017). Petrophysical properties distribution modelling of an onshore field, Niger Delta, Nigeria. *Current Research in Geoscience, 7*(1), 14–24.

Evamy, D. D. J., Haremboure, P., Kamerling, W. A., Knaap, F., Molloy, A.and Rowlands, M. H. (1978). lies within latitude Hydrocarbon habitat of the Tertiary Niger Delta. *American Association of Petroleum Geologists Bulletin, 62*(1), 1–39.

Michele, T., Ronald, C. and Michael, B. (2015). The Niger Delta petroleum system: Niger Delta Province, Nigeria, Cameroon, and Equatorial Guinea, Africa. *United States Geological Survey Report*.

Nwankwo, C. N., Anyanwu, J. and Ugwu, S. A. (2014). Integration of seismic and well log data for petrophysical modeling of sandstone hydrocarbon reservoir in Niger Delta. *Scientia Africana, 13*(1), 186–199.

Reijers, T. J. A. (2011). Stratigraphy and sedimentology of the Niger Delta. *Geologos, 17*(3), 133–162.

Rivenæs, J. C., Sørhaug, P. and Knarud, R. (2015). Introduction to reservoir modelling. In K. Bjørlykke (Ed.), *Petroleum geoscience: From sedimentary environments to rock physics* (2nd ed., pp. [page range]). Springer. https://doi.org/10.1007/978-3-642-34132-8

Short, K. C., and Stauble, J. (1967). Outline geology of the Niger Delta. *American Association of Petroleum Geologists Bulletin, 51*(5), 761–779.

Stacher, P. (1995). Present understanding of the Niger Delta hydrocarbon habitat. In M. N. Oti & G. Postma (Eds.), *Geology of deltas* (pp. 257–268). Rotterdam: A.A. Balkema.

Udegbunam, E. O.and Ndukwe, K. (1988). Rock property correlation for hydrocarbon producing sand of the Niger Delta sand. *Oil and Gas Journal, 86*(2), 11–22.

Uwem, T., Udofia, M., Avwunudiogba, A. and Ugwueze, C. (2018). Characterization of R-8 reservoir zone in Ataga oil field, shallow offshore Niger Delta. *International Basic and Applied Research Journal, 3*(6), 1–13.

Weber, K. J.and Daukoru, E. M. (1975). Petroleum geology of the Niger Delta. *Proceedings of the Ninth World Petroleum Congress, 2*, 210–221

Xiao, H. and Suppe, J. (1992). Origin of rollover. *American Association of Petroleum Geologists Bulletin, 76*(4), 509–229.